ACS APPLIED POLYMER MATERIALS

pubs.acs.org/acsapm

Article

Highly Comfortable and Durable Single-Layer Knitted Textile-Based Triboelectric Nanogenerator for Smart Wearable Applications

Viraj U. Somkuwar,* Sandeep Kumar Maurya, and Bipin Kumar*

Cite This: *ACS Appl. Polym. Mater.* 2024, 6, 407−418

Read Online

ACCESS | Metrics & More | Article Recommendations | Supporting Information

ABSTRACT: Amidst the global quest for sustainable energy solutions, there have been endeavors to revolutionize energy-harvesting methods, opening pathways to innovative approaches that tap into the inherent potential of natural sources. The integrated textile-based triboelectric nanogenerator (T-TENG) offers a viable solution to harness human mechanical energy through the clothing. T-TENG has shown several advantages, including flexibility, lightweight, and conformability, for wearable applications. Herein, knitting engineering is utilized for the precise positioning of triboelectric (nylon and polypropylene (PP)) and electrode materials (copper-blended yarn) within the fabric structure for the fabrication of T-TENG. A combination of rib, single jersey, and derivatives of rib knitting techniques was employed to create different tribo structures, namely, 1R1C, pocket, plating, and ridge. The ridge and plated structures showed the highest performance with a peak power density of 110 and 45 $\mu W/m^2$, respectively. Both structures demonstrated excellent air and water vapor permeability and a stable output up to 12,000 cycles of contact separation with excellent long-term durability. The study strongly affirms that the use of commodity textile materials and modifying the structural features of the knitted fabric have significant potential to produce renewable power sources for wearable electronic gadgets.

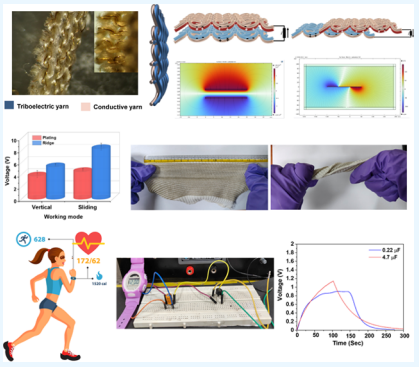

KEYWORDS: *textile triboelectric nanogenerator, knitting, textile structure, renewable energy, energy harvesting, sustainable energy solutions*

INTRODUCTION

In recent years, energy harvesting has garnered significant interest for sustainable power generation. The incorporation of textile-based triboelectric nanogenerators (T-TENGs) presents a practical and sustainable remedy for capturing human biomechanical energy, an underutilized resource within our daily lives that often goes to waste. The TENG converts mechanical energy into electrical energy by harnessing friction induced charge transfer between different materials.[1] Research indicates that an estimated daily output of few milliwatts to several watts of human biomechanical energy remains untapped, highlighting the significance of T-TENGs in converting this overlooked resource into a valuable source of power.[2,3] Traditional power sources, such as batteries, require frequent recharging, leading to a greater environmental impact through increased waste generation, which in turn undermines sustainability efforts. The nonconventional energy-harvesting technologies utilizes unused sources such as kinetic,[4] wind,[5] water,[6] solar,[7] and heat[8] to convert it into electricity or other useable forms. In this quest, researchers have investigated piezoelectric,[9] thermoelectric,[8,10] photovoltaic,[11] electromagnetic,[12] and triboelectric nanogenerators[13] that transform mechanical, thermal, or other sources of ambient energy into the electrical energy. Among the technologies, the triboelectric nanogenerators (TENGs) have drawn immense attraction due to their distinctive benefits, including simple designing, exceptional output performance, remarkable durability, cost-effectiveness in fabrication, and, notably, the capacity to harness abundant mechanical energies encountered in everyday human life.[14−18] Traditionally, TENGs have been designed using rigid and brittle materials, such as metals and polymers, which restricts their flexibility, comfort, and practical implementation.[19−21] Textiles are ubiquitous in our daily lives, possess inherent flexibility, and lightweight making them ideal for harvesting biomechanical energy from the human motion and the friction between fabric layers.[22,23] The amalgamation of smart textiles and TENG brings forth various possibilities for wearable applications such as generating electricity from human movements, enabling self-powered and seamlessly integrated wearable clothing.[19,24] This opens innovative horizons for creating comfortable, interactive, and energy-efficient wearable technology.

Received: September 7, 2023
Revised: December 7, 2023
Accepted: December 13, 2023
Published: December 28, 2023

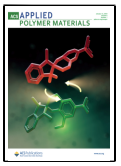

https://doi.org/10.1021/acsapm.3c02087
ACS Appl. Polym. Mater. 2024, 6, 407−418

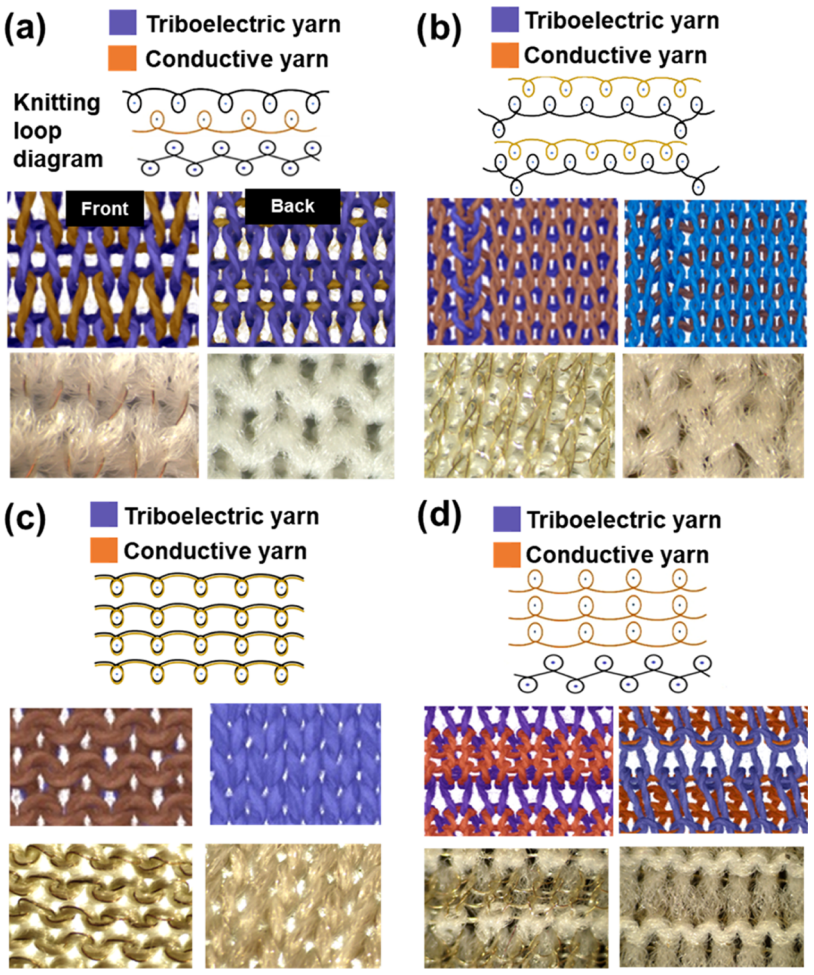

Figure 1. Schematic loop diagram, arrangement of triboelectric and electrode yarn, and the optical images of (a) 1R1C, (b) pocket, (c) plating, and (d) ridge structure.

In T-TENG, the inherent triboelectric characteristics of textile materials make them suitable for charge generation, and the metallic electrode is required for extracting the charge. The metal wire blended yarn,[25,26] metal coated[27] or plated fabric are being used as an electrode material which is integrated using coating,[27] adhesion onto textiles,[28] stitching,[29] sandwiching[24,30] and direct integration.[20,29,31] The textiles are utilized as a substrate for TENGs due to their ability to support the deposition and integration of functional materials.[32,33] There were several different techniques being employed, including layer-by-layer coating,[34] electroless and chemical vapor deposition,[35] and printing.[36] However, this process requires great precision and specialized equipment to support the mass production.[37,38] The stitching and sandwiching process is multistage and time-consuming and deteriorates the flexibility of the garment. Thus, direct integration emerged as a viable solution which offers several advantages such as enhanced flexibility, confirmability, and retaining inherent comfort and breathability of the textile fabric.

Several researchers have explored the weaving,[29,39,40] knitting,[15,17,26] electrospinning,[41] and nonwoven[42,43] manufacturing processes to design an integrated T-TENGs. The woven structure has a straight yarn segment, which restricts the mobility and flexibility. Nonwoven structures lack in mechanical strength and confirmability; hence, it is not a popular choice for wearable applications. In contrast, knitted fabrics, formed by interlooping yarn, offers diverse array of structural elements and their combination, provide a flexible structure and the opportunities to develop an integrated TENGs supporting the industrial textile manufacturing.[44,45] In this direction, several researchers explored tubular structure and three-dimensional (3D) spacer fabric designed using knitting. Although a high TENG output is obtained, however, produces a fabric with an areal density of 7667 g/m^2, which is heavier, thicker, and not suitable for the apparel clothing.[17] In this context, the higher thickness increases the stiffness and deteriorates the comfort characteristics of the fabric.[46] Although the TENG offers promising energy-harvesting capabilities, it is crucial to address the challenges such as comfortability, washability, stability, and durability to ensure optimal user experience and practicality. Fabrics undergo repeated washing, drying, and rigors of everyday use which can affect the performance. Hence, further exploration is needed to determine the feasibility of bulk manufacturing integrated T-TENG that is unobtrusive, comfortable, and suitable for apparel use.

The inherent surface roughness created by the knitted loop plays a significant role in the performance of TENGs as discussed in our previous study.[31] The 3D loop profile produces texture and irregularities on the textile surface thereby improving the effective contact and separation between materials which promote the generation of electro-

https://doi.org/10.1021/acsapm.3c02087
ACS Appl. Polym. Mater. 2024, 6, 407−418

Table 1. Physical Characteristics of the Developed Triboelectric Layers

structure	material	thickness (mm)	loop length (mm)		areal density (g/m^2)	total electrical resistance (Ω)
			Dielectric yarn	Conductive yarn		
pocket	nylon	1.36	4.4	4.4	328	1.4
	PP	1.31	4.7	4.7	317	1.6
1R1C	nylon	1.32	5.4	3.1	215	8.0
	PP	1.29	5.7	3.35	210	8.3
plating	nylon	0.99	4.3	4.3	272	3.2
	PP	1.11	5.1	5.1	281	3.4
ridge	nylon	1.49	8.4	4.21	250	0.6
	PP	1.63	8.7	4.35	220	1.1

static charges.[31] A wide exploration of knitted structures in terms of surface roughness was conducted by sandwiching triboelectric and electrode materials revealing arrangement of face and back loop affects the effective contact area.[15,47] However, the integrated structure has the potential to utilize a wide range of surface roughness and contact areas, necessitating extensive investigation.

In the current research, we describe the development of an integrated T-TENG using knitting technology. The aim of this study was to exploit the potential of utilizing knitting techniques to fabricate TENG structures with improved wearability properties. The wearability parameters, including abrasion resistance, washing stability, comfort properties, and long-term durability, were systematically analyzed to evaluate the performance and feasibility of the developed structures. The energy-harvesting capabilities of the knitted TENGs were successfully demonstrated by charging a capacitor and powering a digital wristwatch. This work showcases the potential of knitting technology for the creation of wearable and sustainable energy-harvesting devices.

EXPERIMENTAL SECTION

Materials. A textured multifilament yarn of nylon and PP with a linear density of 300 denier was used as a triboelectric material. Nylon yarn was employed as the tribo positive material, while PP yarn was utilized as the tribo negative material. Additionally, a copper monofilament yarn of 400 denier was used as the electrode with a linear electrical resistance of 4 Ω/m. The fabrication of a robust T-TENG (textile triboelectric nanogenerator) was done by integration of a copper electrode within four different types of knitted structures.

Fabrication of Integrated TENG. A 14-gauge computerized Flat V-bed knitting machine (SHIMA SEIKI-SVR093SP) was used to prepare the T-TENG samples. The derivatives of rib and single jersey structures were used to produce an integrated TENG structure to keep the triboelectric and conductive yarns on the face and back side of the fabric. Figure 1a–d shows the loop diagram in which the position of the conductive yarn is indicated by an orange color running on the back bed of the knitting machine and a black color triboelectric yarn interlooping on the front and back bed connecting both the layers together. The 1R1C structure was designed using a combination of rib and circular knit structure. The structure produces one course of rib followed by one circular course and hence is denoted as 1R1C (Figure 1a). Tubular knitting produces a two-layer structure that forms a hollow space between the layers (pocket). The combination of a tubular structure with intermittent rib knitting makes a two-layer structure with a vertical interlocking point, thus producing two layers of an integrated single TENG fabric (Figure 1b). The plated structure was developed by knitting the triboelectric and conductive yarns on a single bed simultaneously. Both yarns were supplied with different guide bars to keep their positions relative to the front and back faces of the fabric to achieve a bipartite structure (Figure 1c). A ridge knit fabric structure is defined as a fabric bulge created on the back side of the fabric due to a held loop on one of the beds. In contrast, the other bed continues knitting for a few courses, and then the held loop is transferred onto the working bed (Figure 1d). All of the fabric samples were washed and oven-dried to remove any impurities from the surface followed by conditioning in a standard atmospheric condition (65 % RH and 20 °C) prior to testing.

Characterization of T-TENG. *Structural Characterization and Surface Morphology.* The optical images of the tribo structures were analyzed using an optical microscope. The morphologies of the textile tribo structures were examined using a Zeiss EVO 18 scanning electron microscope (SEM). The image scanning was done by application of a 20 kV acceleration voltage in a vacuum environment. The surface roughness of the samples was analyzed using a 3D optical profiler (Zeta-10, Zeta instrument).

Friction Measurement by a Multifunctional Tribotester. The static and kinetic friction between the tribo layers during the linear sliding mode was determined using the multifunctional tribotester (Rtec Instruments). A friction and wear mode was used with a velocity of 30 mm/s, a stroke length of 5 mm, and a load of 2 N.

Durability and Comfort Analysis. The long-term performance durability assessment was carried out through abrasion resistance testing using a Martindale abrasion and piling tester (Supporting Information, Figure S5a) according to ASTM D4966−12. The samples were rubbed up to 10,000 cycles and the triboelectric performance was assessed after every 2000 cycles. The weight reduction after the abrasion was also calculated to examine the wear loss due to the abrasion. The washing durability was analyzed using a Launder-o-meter (Fastness testing equipment, RB Electronics Eng. Pvt. Ltd., Mumbai, India) as per AATCC TM61. The test was conducted for 10, 20, and 30 washing cycles and the triboelectric performance after every 10 cycles was evaluated.

The air permeabilities of all of the tribo structures were measured using an air permeability instrument with a pressure of 125 Pascal (Supporting Information, Figure S5b). A sample of area 20 cm^2 was taken and the volume of air passing through a unit area of fabric in 1 second was measured as the air permeability value according to ASTM D737−18. The moisture permeability through the fabric was determined using a water vapor permeability (WVTR) tester following ASTM E96 and the rate of moisture in grams transmitted through a meter square fabric in 1 day was measured using the water method.

Electrical Measurements. The triboelectric measurements were done on a sample of size 10 cm × 10 cm in a vertical and horizontal contact separation mode using a separate fabricated mechanism. The open circuit voltage and short circuit current were determined using an oscilloscope (R&S RTB2002) and a Keysight B2985A electrometer with triax cable N1415A. The total resistance of the knitted structures was measured using the 6 1/2 digit precision multimeter (fluke 8846A) with a two-probe technique. The dielectric measurement was done using a Keysight E4980AL LCR meter and 16451B test clamp. All of the electrical parameters were obtained in an EMI-shielded environment chamber (Metrex Scientific Industrial Pvt. Ltd.) with standard ISO 139 atmospheric conditions (20 ± 2 °C, 65 ± 4 % RH). The necessary measures were taken for filtering out the noise in the measurement results and are detailed in the Supporting Information, Figure S1.

https://doi.org/10.1021/acsapm.3c02087
ACS Appl. Polym. Mater. 2024, 6, 407−418

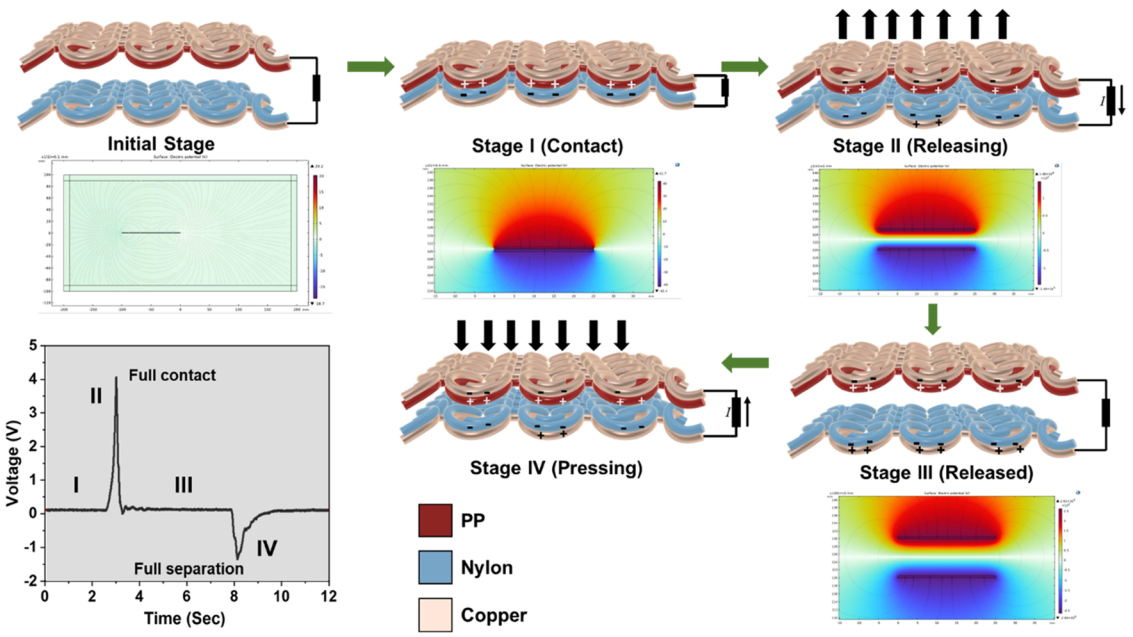

Figure 2. Energy generation cycle of TENG and respective electric output signal in vertical contact separation.

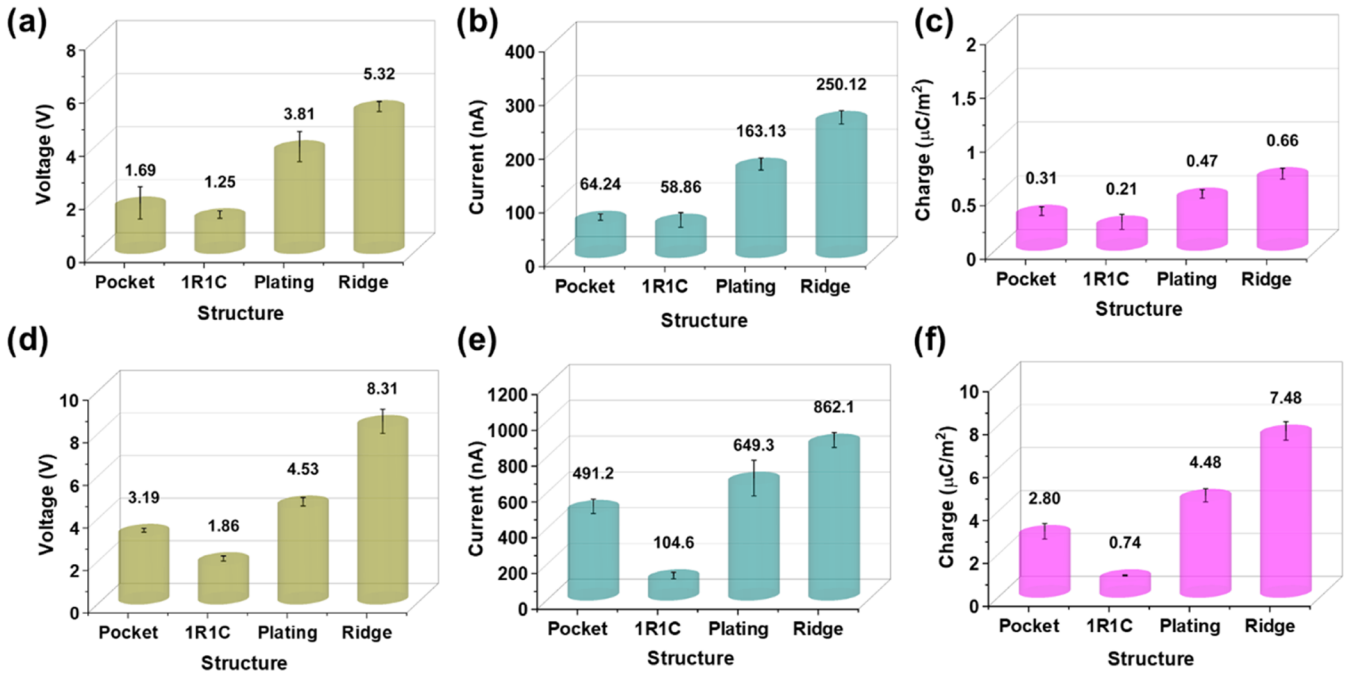

Figure 3. Triboelectric performance (voltage, current, and charge) of different tribo structures under (a−c) vertical contact separation and (d−f) linear sliding mode.

RESULTS AND DISCUSSION

The performance of the TENG device is mainly dependent on the material selection and structural configuration of a conductive and dielectric material. The results have shown varied levels of output performance for the developed tribo structures. The physical specifications, including the thickness, loop length, areal density, and the electrical resistance of the developed fabric samples, are given in Table 1. The thickness and areal density of the fabric are well within the limit of the properties of the apparel garments, indicating its feasibility in wearable applications. The PP ridge structure of TENG showed exceptional lightweight with an areal density of only 209 g/m^2 as compared to the literature where the researchers reported an areal density of 7667 g/m^2 in a PTFE tubular structure and 341 g/m^2 in a warp knitted structure.[17,48] The optical images depict the arrangement of triboelectric yarn on the face and conductive yarn on the back side of the developed tribo structure. The 3D loop arrangement of the knitted structure creates various textures on the fabric surface, which are also visible in the optical images of the tribo structures. The utilization of a textured multifilament yarn enhances the surface roughness and the contact area.

Electrical Performance of T-TENG. The triboelectric measurement was done on a fabricated vertical and sliding

https://doi.org/10.1021/acsapm.3c02087
ACS Appl. Polym. Mater. 2024, 6, 407−418

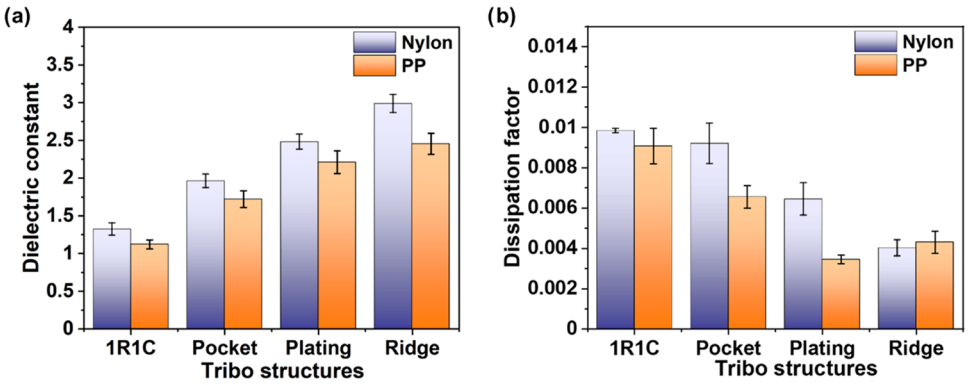

Figure 4. (a) Dielectric constant and (b) dissipation factor of the developed tribo structures.

machine setup controlled by a linear motor actuator. The back-and-forth movement of the movable clamp generates the contact and separation actions between the two triboelectric layers in a vertical direction in tapping and in a horizontal direction in the sliding mechanism. The working mechanism of the nanogenerator in vertical contact separation and sliding mode is illustrated in Figure 2 and Supporting Information, Figure S2. The interaction of triboelectrification and electrostatic induction is demonstrated in different stages of the working cycle. The electron transfer takes place due to contact electrification from the nylon to the PP owing to the difference in their triboelectric properties. A charge imbalance occurs on the two fabrics, with the nylon becoming negatively charged and the PP becoming positively charged relative to each other.[49] The charge imbalance induces free charges on the electrode, which flow through the connected electric circuit (stage II). As the fabrics continue to separate against each other in both working modes, the charge redistribution takes place on the copper electrode due to the electrostatic induction effect. The flow of current ceases as the electric potential reaches an equilibrium, but the surface charge is not annihilated; hence, as the layers start to separate, the system begins to neutralize to recombine the potential difference that flows the current in the opposite direction (Stage IV). The entire power generation cycle, along with the potential distribution, was simulated and illustrated using the COMSOL Multiphysics software, as depicted in Figure 2.

The structural comparison for the output voltage, current, and charge in response to the periodic contact separation of different tribo structures is shown in Figure 3a–f. A contact frequency of 1 Hz and pressure of 25 kPa were used in vertical contact separation mode and a sliding speed of 90 cycle per min was maintained in a sliding mode. The tribo structure—tubular, 1R1C, plating, and ridge—showed an open circuit voltage of 1.69, 1.25, 3.81, and 5.32 V, respectively. The short circuit current and the charge showed, respectively, an improvement of 289 and 113 % for the ridge structure as compared to 1R1C. The voltage and current waveform analysis showed a sharp triangular peak generated during contacting and releasing states due to an instant contact and separation action between the two triboelectric layers, as depicted in Figure 2. In comparison, the lateral sliding mode generated a peak with plateau at the top and bottom (Supporting Information, Figure S2) due to the fabric layers sliding past each other; hence, the contact period is higher as compared to the vertical contact separation mode. As a result, the sliding mode exhibited a better triboelectric performance when compared among all of the tribo structures.

The results of sliding contact separation show a voltage of 1.86 V and a current of 104.6 nA for 1R1C, while the ridge demonstrates a maximum voltage of 8.31 V and a current of 862 nA followed by plating and the pocket as depicted in Figure 3d,e. When compared to vertical contact separation mode, the ridge construction demonstrated a significant improvement of 56 and 245 % in voltage and current, respectively. The improvement can be attributed to the sliding mechanism employed, which facilitates a longer duration of charge transfer, enhancing the efficiency of the system.[48,50] This also results in enhanced charge density of the ridge from 0.66 to 7.48 $\mu C/m^2$ in the sliding mechanism (Figure 3c,f).

The triboelectric performance of TENG is primarily affected by the dielectric characteristics, contact area, surface roughness, frictional properties between the layer, and structural arrangement of the dielectric and conductive components in the system.[31,51,52] The aforementioned parameters were evaluated using different characterization techniques. The dielectric and dissipation factors of individual tribo structures are depicted in Figure 4. The ridge structure showed higher dielectric constants of 2.46 and 2.98, whereas 1R1C exhibited the lowest values of 1.12 and 1.32 for PP and the nylon fabric, respectively. The higher dielectric constant of the ridge structure is due to its higher thickness as compared to the other structures (Table 1). The low dissipation factor implies that there is minimal energy loss during the charge transfer process. As a result, more energy is effectively transferred, leading to higher voltage and current levels. Hence, the combination of higher dielectric constant and lower dissipation realized maximum triboelectric output for the ridge structure.[53,54]

The contact area has a direct correlation with the triboelectric output as the charge separation is caused by the surface contact.[31,55,56] The surface roughness evaluation was carried out to predict the surface contact between the two tribo layers. The surface textures of the tribo structures were determined by the formation of the peaks and valleys created by the 3D configuration of the knitted loop profile. The color map and 3D profile of the knitted structures are depicted in Supporting Information, Figures S3 and S4. The mean surface roughness (S_a) of 218, 102, 190, and 391 μm was measured for 1R1C, pocket, plating, and ridge nylon structure, respectively, whereas the structures made with PP as triboelectric yarn showed a mean surface roughness of 186, 150, 185, and 462 μm for 1R1C, pocket, plating, and ridge nylon structure,

https://doi.org/10.1021/acsapm.3c02087
ACS Appl. Polym. Mater. 2024, 6, 407−418

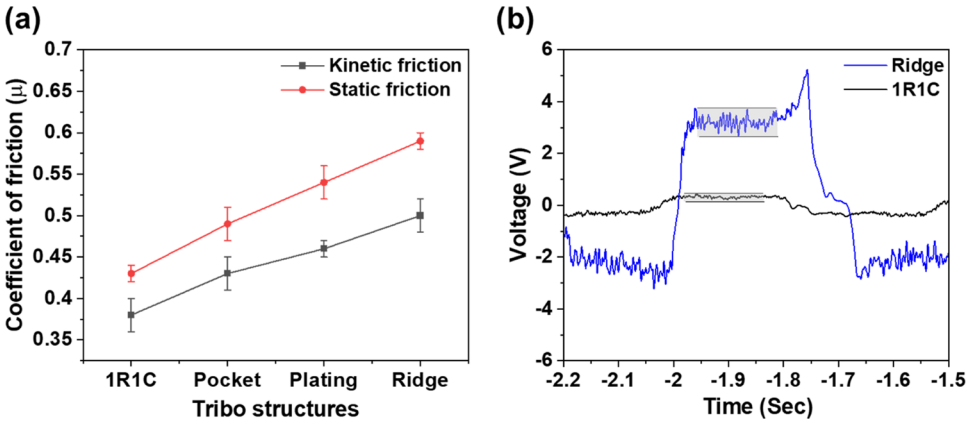

Figure 5. (a) Static and kinetic coefficients of friction among different pairs of tribo structures. (b) Enlarged voltage waveforms of the ridge and 1R1C structures depicting multiple macrocontact separations at the top of the peak.

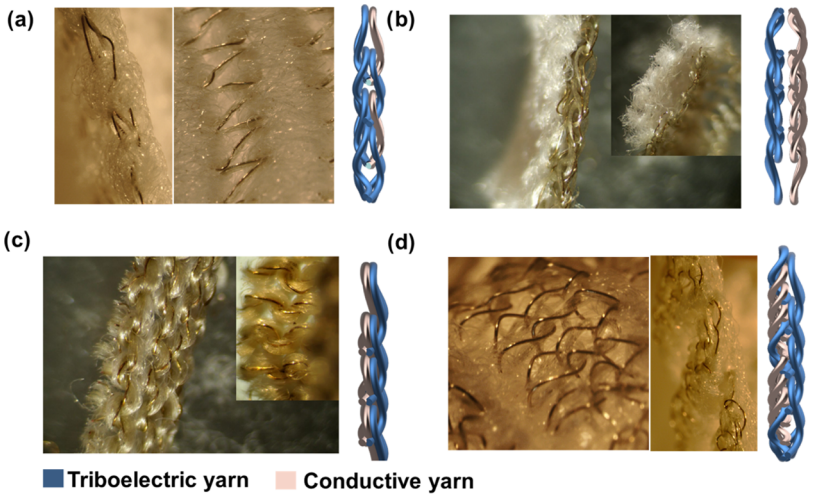

Figure 6. Illustrations showing dielectric to conductive contact between the (a) 1R1C, (b) pocket, (c) plating, and (d) ridge tribo structure.

respectively. The higher surface roughness of nylon and PP ridge tribo structures yielded a notable increase in contact area when used in pair in the TENG performance measurement. The surface roughness of the tribo structures indicates the static and kinetic frictions between the contacting triboelectric layers, while the higher surface roughness also contributed enhanced surface contact area, consequently resulting in a higher voltage output.[57,58]

Figure 5a illustrates the static and kinetic friction data for the designed tribo structure pairs determined using the tribotester. The ridge structure showed static and kinetic coefficients of friction (μ) of 0.59 and 0.50, respectively, which are the highest among all of the tribo structures due to its higher surface roughness. The high friction leads to enhanced contact area, which increases the induced charged density between the contacting surfaces.[50,59] The frictional restraint during the sliding mode triggered multiple microcontact separation cycles while two triboelectric layers are sliding past each other. It has been reported that the coefficient of friction between the contacting materials has a correlation with the nature of the sliding output signal.[50,59] The different amplitudes and wavelengths of the multiple microcontact separation cycles were observed at the top and bottom of the output signal in sliding mode for the developed tribo structures 1R1C and Ridge as described in Figure 5b.

The magnitude of contact between the dielectric and conductive materials affects the nature of electrostatic induction and charge flowing through the electrodes.[13,60] This assumption is verified from the arrangement of the dielectric and conductive yarn in different tribo structures and their output results. The 1R1C structure comprised a single conductive yarn course for every two dielectric courses. Hence, minimal contact between the two types of yarns is observed. However, the ridge structures have three courses of conductive yarns contacting each dielectric course, resulting in a higher dielectric to conducive contact. Similarly, the plated structure knit the triboelectric and conductive yarns together at each course, delivering a higher output voltage, current, and charge than the tubular and 1R1C tribo structures (Figure 6). The interlooping of the conductive and dielectric yarn also forms a resistive network that influences the total resistance of the yarn affecting the charge flowing through the conductor. The variations in resistance values among the four types of knitted fabrics can be attributed to the length and contact resistance.[61] A single course of conductive yarn produces a length resistance proportional to the length of a conductive course and the intrinsic resistance of the conductive element. A contact resistance forms by the overlapped yarns at the crossover points between two consecutive courses and wales. The 1R1C fabric had the highest resistance value due to a single course of

https://doi.org/10.1021/acsapm.3c02087
ACS Appl. Polym. Mater. 2024, 6, 407−418

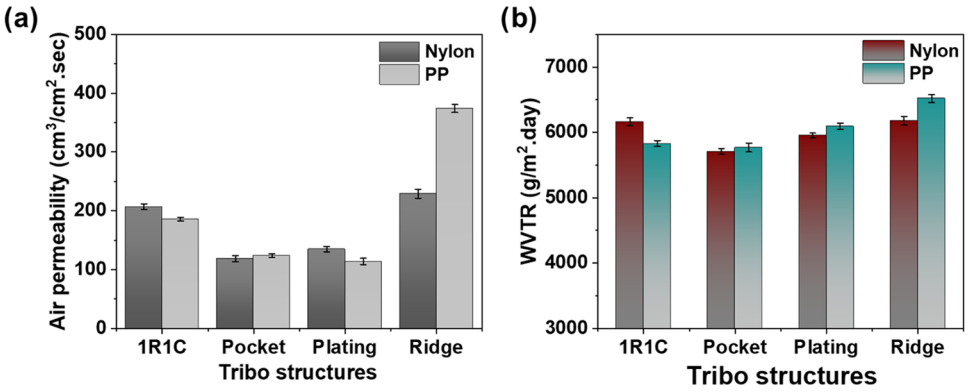

Figure 7. (a) Air permeability and (b) water vapor permeability of the designed tribo structures.

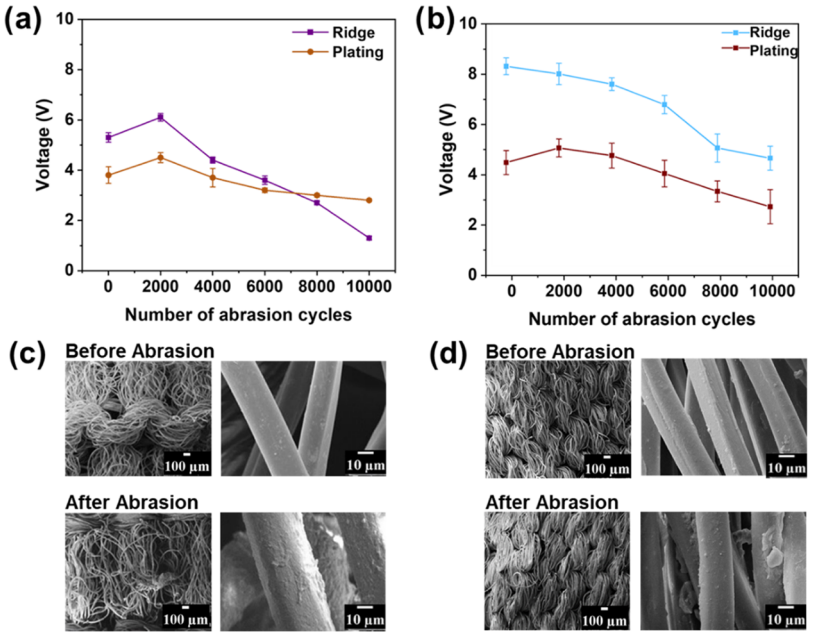

Figure 8. Effect of abrasion resistance testing of ridge and plated tribo structures on the output voltage in (a) vertical and (b) linear sliding contact separation mode, and the surface damage assessment through SEM before and after the abrasion of 10,000 cycles for (c) ridge and (d) plated tribo structure.

conductive yarn, which results in a longer path for the current to flow. Consequently, the ridge fabric had the lowest resistance value due to the higher density of the consecutive conductive coarses imparting a lower contact resistance.

Durability and Comfort Assessment. Comfort assessment was carried out using the air and water vapor permeability measurement. The results showed excellent air permeability due to the knit loop configuration of all of the structures, indicating its better comfort performance (Figure 7a). The ridge knitted structure stands out for its exceptional air permeability, surpassing all other tribo structures and the existing developed textile TENGs.[62] Similarly, the ridge structure shows excellent water vapor permeability of up to 6500 g/m^2·day (Figure 7b).

Since the ridge and plating structures showed excellent TENG performance as compared to other structures, the long-term durability was evaluated for these structures. The frequent friction during the contact separation mechanism of TENG exerts rigorous forces on the fabric surface, creating micro- and macro-level damage to the surface. To analyze the effect of damage during the rubbing of the TENG layers, the abrasion resistance of the tribo structures was tested for 10,000 cycles followed by electrical measurement in vertical and sliding contact separation modes. The triboelectric performance was gradually reduced during the abrasion testing for ridge and plated structures. The voltage and current showed an initial improvement until 2000 cycles, then they decreased gradually as the number of rubbing cycles were increased when tested in vertical contact separation mode. The initial improvement was attributed to the increased surface roughness due to interfacial friction. The initial reduction after 4000 cycles was 16 %, and then further the voltage was significantly reduced up to 70 % after the abrasion of 10,000 cycles in the case of ridge structure. A similar trend was observed in linear sliding mode with an overall reduction of 45 % in voltage (Figure 8a,b). After comparing the ridge and plated tribo structures, the deterioration of TENG performance after the abrasion was found to be more pronounced in the ridge. The contacting surface of the ridge structure features a held loop that loosely binds the constituent filaments, making them more susceptible to damage during the abrasion process. In contrast, the plated knit structure is produced by knitting two yarns simultaneously

https://doi.org/10.1021/acsapm.3c02087
ACS Appl. Polym. Mater. 2024, 6, 407−418

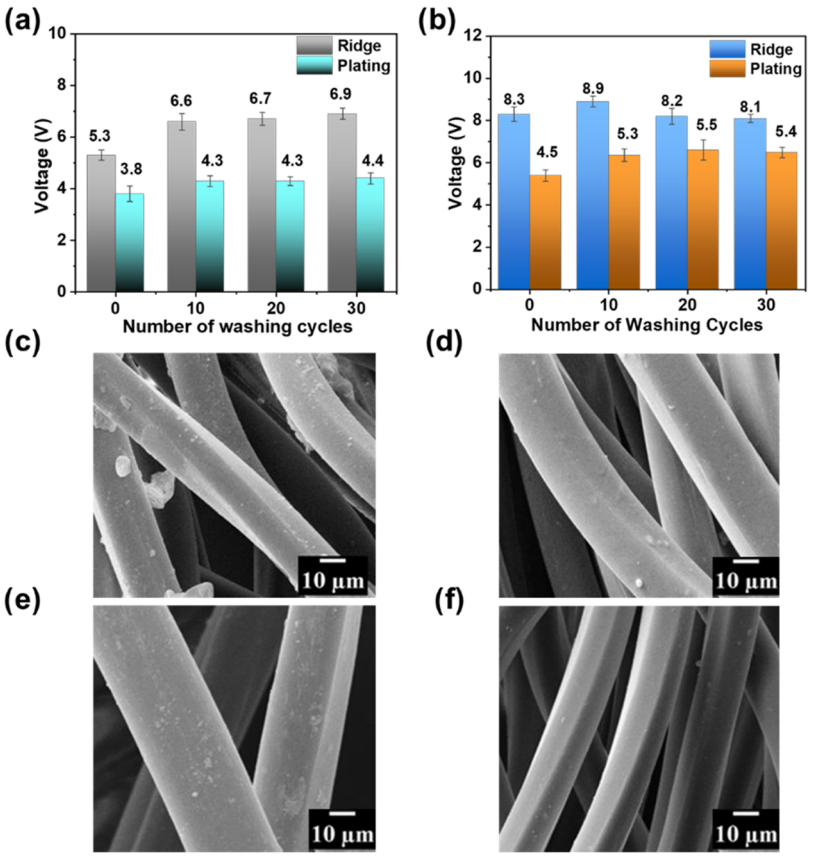

Figure 9. Effect of washing durability on voltage of (a) vertical contact separation mode, (b) lateral sliding mode, and SEM images of (c, d) PP, and (e, f) nylon before and after the washing treatment.

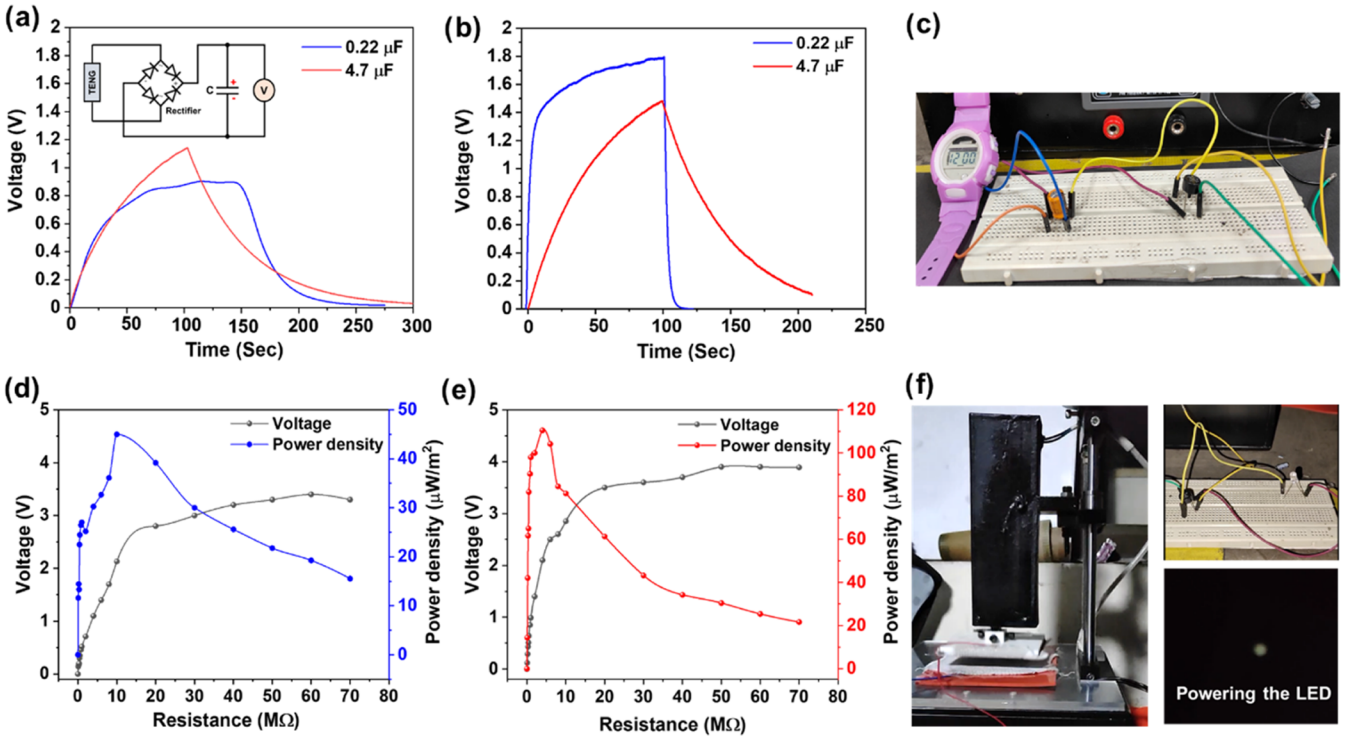

Figure 10. Capacitor charge−discharge pattern of (a) plating (inset showing circuit connections) and (b) ridge tribo structure with different capacitors (0.22 and 4.7 μF). (c) A digital wristwatch driven by the 4.7 μF capacitor while discharging. The peak power density of (d) plating and (e) ridge tribo structures at different load resistances. (f) Photograph of the TENG setup for powering the LED.

https://doi.org/10.1021/acsapm.3c02087
ACS Appl. Polym. Mater. 2024, 6, 407−418

Table 2. Comparison of Comfort and Stability Performances of the Existing and Current Studies[a]

structure	areal density (g/m^2)	no. of cycles: stability	no. of cycles: abrasion	no. of cycles: washing	air permeability (mm/s)	WVTR (g/m^2·day)	refs
tubular	7667.4	6000		10	1491		17
laminated knit fabric		500		10	884.78		63
printed knitted fabric		14,400			1010 (101 cm^3/cm^2/s)		62
warp knitted terry fabric	341	10,000	2500		800−900		64
rib knitted fabric		10,000			600 mm/s (6000 L/m^2/s)	960	65
knitted TENG			5000	20	1035−1430	14	66
knitted TENG	220−328	12,000	10,000	30	20000−37500 (200−375 cm^3/cm^2·s)	5000−6000	our study

[a]The air permeability values are converted into mm/sec for comparison; the actual values are shown in the brackets below.

on a single needle bed, hence producing a compact structure. The higher weight loss (%) and the damage depicted in the SEM images of the fabric surface (Supporting Information, Table S1) confirm the higher susceptibility of the ridge structure to abrasion. Subsequently, the SEM image analysis reveals that the ridge structure of the PP and nylon is completely distorted, with multiple broken filaments and damage observed on the filament surface as depicted in Figure 8c. In contrast, the plated structure displayed minimum distortion and no damage to the filament surface during abrasion until 10000 cycles, displaying its good stability in wear-related applications (Figure 8d). The dielectric constant of the fabric was also analyzed to check the change in the charge accumulation behavior after the abrasion. A reduction in the dielectric constant was observed after the abrasion of fabric due to the surface deterioration affecting the charge storage capacity of the fabric (Supporting Information, Figure S7).

The washing durability was evaluated for the ridge and plated structure using the Launder-o-meter. An anionic detergent was used as the washing agent to avoid any detrimental effects on the charge generation behavior of the textile TENG. Each washing cycle comprised a 10 min wash followed by a 5 min hot air-drying period. This sequence was repeated for a total of 30 times. The voltage and current generated were measured and recorded after every 10 cycles. The performance of the tribo structures showed a slight enhancement after washing. The voltage and current were improved, which can be attributed to the removal of surface contamination[17] increasing the effectiveness of contact electrification and thereby increasing the output (Figure 9a−d).

The long-term stability of the plated and ridge knitted TENG was assessed in lateral sliding and vertical modes for 12,000 contact separation cycles. Both structures showed a very stable long-term output with a contact frequency of 1 Hz and pressure of 25 kPa when tested in the vertical contact separation mode as depicted in Supporting Information, Figure S6a, and a sliding speed of 90 cycles per min (Figure S6b).

Application Potential of Textile TENG. The charge generation efficiency of the textile TENG was assessed by the charge−discharge behavior of a capacitor connected through a full wave bridge rectifier in a circuit as shown in the inset of Figure 10a. The charging behavior of a ridge and plated structure was investigated using capacitors of 0.22 and 4.7 μF in the vertical contact separation mode. During the charging period, the capacitors gradually accumulated charge for a constant duration of 100 s, leading to an increase in voltage. Subsequently, the discharging curve was obtained by disconnecting the voltage source, causing the capacitors to release the stored charge and exhibit a voltage decrease. The charging and discharging speeds were gradually reduced as the capacitance of the capacitor was increased. The charge−discharge curve depicted in Figure 10a illustrates the capacitor of 0.22 and 4.7 μF charged to 900 mV and 1.13 V, respectively, for the plated structure. However, the ridge structure charged the capacitor of 0.22 and 4.7 μF to 1.8 and 1.5 V, respectively, in 100 s (Figure 10b). The discharge curve exhibits a sudden reduction in the voltage for a 0.22 μF capacitor, whereas a 4.7 μF capacitor holds the charge for a longer duration for ridge and plated tribo structures. The charge stored in the capacitor showed the potential to power a commercial wristwatch, as demonstrated in Figure 10c and Supporting, Movie S1. The peak power delivered by TENG was measured by connecting different load resistances from 1 KΩ to 100 MΩ in series through the full wave bridge rectifier. In practical application, TENG can deliver the highest power at a specific load resistance, which is equal to its internal resistance. The voltage shows an initial increment with the resistance and gets saturated at the load resistance of 40 MΩ and remains constant until 80 MΩ, as shown in Figure 10d,e. The peak power density for plated and ridge TENG reached 45 and 110 μW/m^2 at a load resistance of 4 and 10 MΩ, respectively. The power density can be calculated using eq 1, where V is the output voltage corresponding to the load resistor R and the contact area of the fabric is denoted by A. The different levels of power density for the plated and ridge tribo structures suggest that they can be used to power the devices having different load capacities. The generated power is also directly utilized to power an LED through the vertical contact separation mechanism with a frequency of 5 Hz. Figure 10f shows that the device can light the LED using the developed fabric TENG without charging the capacitor and the recording of the demonstration of flashing the LED is given in Supporting Information, Movie S2. The application demonstrations illustrate the versatility of the developed textile TENG for different applications with and without the energy storage attachment.

$$\text{peak power density } (\mu\text{W/m}^2) = \frac{V^2}{R \times A} \quad (1)$$

CONCLUSIONS

In summary, an integrated knitted textile TENG was developed using an industrial knitting machine and its ability to harvest the biomechanical energy was demonstrated. The materials utilized in the TENG textiles are well suited for clothing applications as they possess washability, flexibility, breathability, and comfort properties. Four different structures

https://doi.org/10.1021/acsapm.3c02087
ACS Appl. Polym. Mater. 2024, 6, 407−418

were developed with varying components, and their performance was evaluated under the lateral sliding and vertical contact separation mode. The plated and ridge structures demonstrated superior performance, generating peak power densities of 45 and 110 $\mu W/m^2$, respectively. Their enhanced performance can be attributed to the enhanced surface roughness and increased contact area. The sliding mode exhibited a higher output as compared to the vertical contact separation mode, owing to prolonged friction and multiple microcontact separations. The structures displayed impressive long-term stability, enduring a stable output until 12,000 cycles of contact separation and 30 washing cycles. The comparison of durability and comfort properties among the existing studies (Table 2) showed the superior performance of the present study. TENG proved to be a viable power source, as evidenced by successfully powering a digital wristwatch and lighting an LED using the generated power. The developed integrated knitted textile TENG holds promising prospects for future applications in wearable electronics, smart textiles, and self-powered sensors.

■ ASSOCIATED CONTENT

Supporting Information

The Supporting Information is available free of charge at https://pubs.acs.org/doi/10.1021/acsapm.3c02087.

Detailed experimental procedure of current and voltage measurement and effect of abrasion on dielectric constant (PDF)

Demonstration of powering the digital wristwatch driven by the 4.7 μF capacitor while discharging (Movie S1) (MP4)

Demonstration of lightening an LED from the ridge tribo structure under vertical contact separation mode (Movie S2) (MP4)

■ AUTHOR INFORMATION

Corresponding Authors

Viraj U. Somkuwar − *Department of Textile and Fiber Engineering, Indian Institute of Technology Delhi, Delhi 110016, India*; Phone: +91-9727707962; Email: Viraj.Uttamrao.Somkuwar@textile.iitd.ac.in, virajsomkuwar@yahoo.in

Bipin Kumar − *Department of Textile and Fiber Engineering, Indian Institute of Technology Delhi, Delhi 110016, India*; orcid.org/0000-0002-9754-8210; Phone: +91-11-26597240; Email: Bipin.Kumar@textile.iitd.ac.in, bipiniitd18@gmail.com, bipin@textile.iitd.ac.in; Fax: +91-11-26581103

Author

Sandeep Kumar Maurya − *Department of Textile and Fiber Engineering, Indian Institute of Technology Delhi, Delhi 110016, India*

Complete contact information is available at: https://pubs.acs.org/10.1021/acsapm.3c02087

Author Contributions

The manuscript was written through contributions of all authors. All authors have given approval to the final version of the manuscript.

Funding

Funding support was provided by National Technical Textiles Mission, Ministry of Textiles India (Project no.- RP04310G).

Notes

The authors declare no competing financial interest.

■ ACKNOWLEDGMENTS

The author acknowledges CRF and NRF in the Indian Institute of Technology, Delhi for providing research facilities.

■ REFERENCES

(1) Gao, H.; Hu, M.; Ding, J.; Xia, B.; Yuan, G.; Sun, H.; Xu, Q.; Zhao, S.; Jiang, Y.; Wu, H.; et al. Investigation of contact electrification between 2D MXenes and MoS2 through density functional theory and triboelectric probes. *Adv. Funct. Mater.* **2023**, *33* (15), No. 2213410.

(2) Choi, Y.-M.; Lee, M. G.; Jeon, Y. Wearable Biomechanical Energy Harvesting Technologies. *Energies* **2017**, *10* (10), No. 1483, DOI: 10.3390/en10101483.

(3) Riemer, R.; Shapiro, A. Biomechanical energy harvesting from human motion: theory, state of the art, design guidelines, and future directions. *J. Neuroeng. Rehabil.* **2011**, *8*, No. 22, DOI: 10.1186/1743-0003-8-22.

(4) Gang, X.; Guo, Z. H.; Cong, Z.; Wang, J.; Chang, C.; Pan, C.; Pu, X.; Wang, Z. L. Textile triboelectric nanogenerators simultaneously harvesting multiple "high-entropy" kinetic energies. *ACS Appl. Mater. Interfaces* **2021**, *13* (17), 20145−20152.

(5) He, L.; Zhang, C.; Zhang, B.; Yang, O.; Yuan, W.; Zhou, L.; Zhao, Z.; Wu, Z.; Wang, J.; Wang, Z. L. A dual-mode triboelectric nanogenerator for wind energy harvesting and self-powered wind speed monitoring. *ACS Nano* **2022**, *16* (4), 6244−6254.

(6) Ye, C.; Liu, D.; Peng, X.; Jiang, Y.; Cheng, R.; Ning, C.; Sheng, F.; Zhang, Y.; Dong, K.; Wang, Z. L. A hydrophobic self-repairing power textile for effective water droplet energy harvesting. *ACS Nano* **2021**, *15* (11), 18172−18181.

(7) Abdin, Z.; Alim, M. A.; Saidur, R.; Islam, M. R.; Rashmi, W.; Mekhilef, S.; Wadi, A. Solar energy harvesting with the application of nanotechnology. *Renewable Sustainable Energy Rev.* **2013**, *26*, 837−852.

(8) Ryu, H.; Yoon, H. J.; Kim, S. W. Hybrid energy harvesters: toward sustainable energy harvesting. *Adv. Mater.* **2019**, *31* (34), No. 1802898.

(9) Banerjee, S.; Bairagi, S.; Ali, S. W. A lead-free flexible piezoelectric-triboelectric hybrid nanogenerator composed of uniquely designed PVDF/KNN-ZS nanofibrous web. *Energy* **2022**, *244*, No. 123102.

(10) Korkmaz, S.; Kariper, İ. A. Pyroelectric nanogenerators (PyNGs) in converting thermal energy into electrical energy: Fundamentals and current status. *Nano Energy* **2021**, *84*, No. 105888.

(11) Wu, Y.; Qu, J.; Chu, P. K.; Shin, D.-M.; Luo, Y.; Feng, S.-P. Hybrid photovoltaic-triboelectric nanogenerators for simultaneously harvesting solar and mechanical energies. *Nano Energy* **2021**, *89*, No. 106376.

(12) Zhang, C.; Tang, W.; Han, C.; Fan, F.; Wang, Z. L. Theoretical comparison, equivalent transformation, and conjunction operations of electromagnetic induction generator and triboelectric nanogenerator for harvesting mechanical energy. *Adv. Mater.* **2014**, *26* (22), 3580−3591.

(13) Fan, F.-R.; Tian, Z.-Q.; Wang, Z. L. Flexible triboelectric generator. *Nano Energy* **2012**, *1* (2), 328−334.

(14) Wang, W.; Yu, A.; Liu, X.; Liu, Y.; Zhang, Y.; Zhu, Y.; Lei, Y.; Jia, M.; Zhai, J.; Wang, Z. L. Large-scale fabrication of robust textile triboelectric nanogenerators. *Nano Energy* **2020**, *71*, No. 104605.

(15) Kwak, S. S.; Kim, H.; Seung, W.; Kim, J.; Hinchet, R.; Kim, S.-W. Fully stretchable textile triboelectric nanogenerator with knitted fabric structures. *ACS Nano* **2017**, *11* (11), 10733−10741.

(16) Wang, W.; Yu, A.; Zhai, J.; Wang, Z. L. Recent progress of functional fiber and textile triboelectric nanogenerators: towards

electricity power generation and intelligent sensing. *Adv. Fiber Mater.* **2021**, *3* (6), 394−412.
(17) Dong, S.; Xu, F.; Sheng, Y.; Guo, Z.; Pu, X.; Liu, Y. Seamlessly knitted stretchable comfortable textile triboelectric nanogenerators for E-textile power sources. *Nano Energy* **2020**, *78*, No. 105327.
(18) Xu, Q.; Fang, Y.; Jing, Q.; Hu, N.; Lin, K.; Pan, Y.; Xu, L.; Gao, H.; Yuan, M.; Chu, L.; et al. A portable triboelectric spirometer for wireless pulmonary function monitoring. *Biosens. Bioelectron.* **2021**, *187*, No. 113329.
(19) Zhang, H.; Zhang, J.; Hu, Z.; Quan, L.; Shi, L.; Chen, J.; Xuan, W.; Zhang, Z.; Dong, S.; Luo, J. Waist-wearable wireless respiration sensor based on triboelectric effect. *Nano Energy* **2019**, *59*, 75−83.
(20) Yang, W.; Chen, J.; Zhu, G.; Yang, J.; Bai, P.; Su, Y.; Jing, Q.; Cao, X.; Wang, Z. L. Harvesting energy from the natural vibration of human walking. *ACS Nano* **2013**, *7* (12), 11317−11324.
(21) Mi, H.-Y.; Jing, X.; Wang, Y.; Shi, X.; Li, H.; Liu, C.; Shen, C.; Turng, L.-S.; Gong, S. Poly [(Butyl acrylate)-co-(butyl methacrylate)] as Transparent Tribopositive Material for High-Performance Hydrogel-Based Triboelectric Nanogenerators. *ACS Appl. Polym. Mater.* **2020**, *2* (11), 5219−5227.
(22) Paosangthong, W.; Torah, R.; Beeby, S. Recent progress on textile-based triboelectric nanogenerators. *Nano Energy* **2019**, *55*, 401−423.
(23) Ismar, E.; Bahadir, S. K.; Kalaoglu, F.; Koncar, V. Futuristic clothes: electronic textiles and wearable technologies. *Global Challenges* **2020**, *4* (7), No. 1900092, DOI: 10.1002/gch2.201900092.
(24) Lin, Z.; Yang, J.; Li, X.; Wu, Y.; Wei, W.; Liu, J.; Chen, J.; Yang, J. Large-scale and washable smart textiles based on triboelectric nanogenerator arrays for self-powered sleeping monitoring. *Adv. Funct. Mater.* **2018**, *28* (1), No. 1704112.
(25) Maurya, S. K.; Das, A.; Kumar, N.; Kumar, B. Electrothermal and Mechanical Characterization of Stainless Steel and Silver-Coated Cabled Yarns for Heating Application. *ACS Appl. Eng. Mater.* **2023**, *1* (3), 983−993.
(26) Rezaei, J.; Nikfarjam, A. Rib stitch knitted extremely stretchable and washable textile triboelectric nanogenerator. *Adv. Mater. Technol.* **2021**, *6* (4), No. 2000983.
(27) Zhao, Z.; Huang, Q.; Yan, C.; Liu, Y.; Zeng, X.; Wei, X.; Hu, Y.; Zheng, Z. Machine-washable and breathable pressure sensors based on triboelectric nanogenerators enabled by textile technologies. *Nano Energy* **2020**, *70*, No. 104528.
(28) Jian, G.; Meng, Q.; Jiao, Y.; Feng, L.; Shao, H.; Wang, F.; Meng, F. Hybrid PDMS-TiO2-stainless steel textiles for triboelectric nanogenerators. *Chem. Eng. J.* **2021**, *417*, No. 127974.
(29) Somkuwar, V. U.; Pragya, A.; Kumar, B. Structurally engineered textile-based triboelectric nanogenerator for energy harvesting application. *J. Mater. Sci.* **2020**, *55* (12), 5177−5189.
(30) Xiong, J.; Cui, P.; Chen, X.; Wang, J.; Parida, K.; Lin, M.-F.; Lee, P. S. Skin-touch-actuated textile-based triboelectric nanogenerator with black phosphorus for durable biomechanical energy harvesting. *Nat. Commun.* **2018**, *9* (1), No. 4280.
(31) Somkuwar, V. U.; Kumar, B. Influence of the Fabric Topology on the Performance of a Textile-Based Triboelectric Nanogenerator for Self-Powered Monitoring. *ACS Appl. Polym. Mater.* **2023**, *5* (4), 2323−2335.
(32) Choi, D.; Lee, Y.; Lin, Z.-H.; Cho, S.; Kim, M.; Ao, C. K.; Soh, S.; Sohn, C.; Jeong, C. K.; Lee, J.; et al. Recent Advances in Triboelectric Nanogenerators: From Technological Progress to Commercial Applications. *ACS Nano* **2023**, *17* (12), 11087−11219.
(33) Chen, C.; Guo, H.; Chen, L.; Wang, Y.-C.; Pu, X.; Yu, W.; Wang, F.; Du, Z.; Wang, Z. L. Direct current fabric triboelectric nanogenerator for biomotion energy harvesting. *ACS Nano* **2020**, *14* (4), 4585−4594.
(34) Menge, H. G.; Jo, S. H.; Park, Y. T. Layer-by-layer self-assembled thin films for triboelectric energy harvesting under harsh conditions. *ACS Appl. Electron. Mater.* **2021**, *3* (12), 5475−5482.
(35) Huang, X.; Qi, Y.; Bu, T.; Li, X.; Liu, G.; Zeng, J.; Fan, B.; Zhang, C. Overview of Advanced Micro-Nano Manufacturing Technologies for Triboelectric Nanogenerators. *Nanoenergy Adv.* **2022**, *2* (4), 316−343.
(36) Li, H.; Wang, S.; Dong, X.; Ding, X.; Sun, Y.; Tang, H.; Lu, Y.; Tang, Y.; Wu, X. Recent advances on ink-based printing techniques for triboelectric nanogenerators: Printable inks, printing technologies and applications. *Nano Energy* **2022**, *101*, No. 107585, DOI: 10.1016/j.nanoen.2022.107585.
(37) Bai, Z.; Zhang, Z.; Li, J.; Guo, J. Textile-based triboelectric nanogenerators with high-performance via optimized functional elastomer composited tribomaterials as wearable power source. *Nano Energy* **2019**, *65*, No. 104012.
(38) Zhou, M.; Xu, F.; Ma, L.; Luo, Q.; Ma, W.; Wang, R.; Lan, C.; Pu, X.; Qin, X. Continuously fabricated nano/micro aligned fiber based waterproof and breathable fabric triboelectric nanogenerators for self-powered sensing systems. *Nano Energy* **2022**, *104*, No. 107885.
(39) Chen, J.; Guo, H.; Pu, X.; Wang, X.; Xi, Y.; Hu, C. Traditional weaving craft for one-piece self-charging power textile for wearable electronics. *Nano Energy* **2018**, *50*, 536−543.
(40) Yu, A.; Pu, X.; Wen, R.; Liu, M.; Zhou, T.; Zhang, K.; Zhang, Y.; Zhai, J.; Hu, W.; Wang, Z. L. Core−shell-yarn-based triboelectric nanogenerator textiles as power cloths. *ACS Nano* **2017**, *11* (12), 12764−12771.
(41) Jang, S.; Kim, Y.; Lee, S.; Oh, J. H. Optimization of electrospinning parameters for electrospun nanofiber-based triboelectric nanogenerators. *Int. J. Precis. Eng. Manuf.-Green Technol.* **2019**, *6*, 731−739.
(42) Oh, H. J.; Bae, J. H.; Park, Y. K.; Song, J.; Kim, D. K.; Lee, W.; Kim, M.; Heo, K. J.; Kim, Y.; Kim, S. H.; et al. A highly porous nonwoven thermoplastic polyurethane/polypropylene-based triboelectric nanogenerator for energy harvesting by human walking. *Polymers* **2020**, *12* (5), No. 1044, DOI: 10.3390/polym12051044.
(43) Yar, A. High performance of multi-layered triboelectric nanogenerators for mechanical energy harvesting. *Energy* **2021**, *222*, No. 119949.
(44) Maurya, S. K.; Somkuwar, V. U.; Das, A.; Kumar, N.; Kumar, B. Influence of Knitting Engineering and Environment Conditions on the Performance of Heating Textiles for Therapeutic Applications. *ACS Appl. Eng. Mater.* **2023**, *1* (6), 1644−1654.
(45) Maurya, S. K.; Somkuwar, V. U.; Garg, H.; Das, A.; Kumar, B. Thermal protective performance of single-layer rib-knitted structure and its derivatives under radiant heat flux. *J. Ind. Text.* **2022**, *51*, 8865S−8883S, DOI: 10.1177/15280837211042680.
(46) Li, M.; Xu, B.; Li, Z.; Gao, Y.; Yang, Y.; Huang, X. Toward 3D double-electrode textile triboelectric nanogenerators for wearable biomechanical energy harvesting and sensing. *Chem. Eng. J.* **2022**, *450*, No. 137491.
(47) Niu, L.; Miao, X.; Li, Y.; Xie, X.; Wen, Z.; Jiang, G. Surface Morphology Analysis of Knit Structure-Based Triboelectric Nanogenerator for Enhancing the Transfer Charge. *Nanoscale Res. Lett.* **2020**, *15* (1), No. 181, DOI: 10.1186/s11671-020-03401-1.
(48) Wang, T.; Shen, Y.; Chen, L.; Wang, K.; Niu, L.; Liu, G.; He, H.; Cong, H.; Jiang, G.; Zhang, Q.; et al. Large-scale production of the 3D warp knitted terry fabric triboelectric nanogenerators for motion monitoring and energy harvesting. *Nano Energy* **2023**, *109*, No. 108309.
(49) Veeralingam, S.; Badhulika, S. Ti@MoS2 incorporated Polypropylene/Nylon fabric-based porous, breathable triboelectric nanogenerator as respiration sensor and ammonia gas sensor applications. *Sens. Actuators, B* **2023**, *380*, No. 133346.
(50) Zhang, W.; Diao, D.; Sun, K.; Fan, X.; Wang, P. Study on friction-electrification coupling in sliding-mode triboelectric nanogenerator. *Nano Energy* **2018**, *48*, 456−463.
(51) Lin, L.; Xie, Y.; Niu, S.; Wang, S.; Yang, P.-K.; Wang, Z. L. Robust triboelectric nanogenerator based on rolling electrification and electrostatic induction at an instantaneous energy conversion efficiency of∼ 55%. *ACS Nano* **2015**, *9* (1), 922−930.
(52) Zhang, R.; Olin, H. Material choices for triboelectric nanogenerators: a critical review. *EcoMat* **2020**, *2* (4), No. e12062.

(53) Ippili, S.; Jella, V.; Thomas, A. M.; Yoon, C.; Jung, J.-S.; Yoon, S.-G. ZnAl−LDH-induced electroactive β-phase and controlled dielectrics of PVDF for a high-performance triboelectric nanogenerator for humidity and pressure sensing applications. *J. Mater. Chem. A* **2021**, *9* (29), 15993−16005.
(54) Peng, Z.; Xiao, X.; Song, J.; Libanori, A.; Lee, C.; Chen, K.; Gao, Y.; Fang, Y.; Wang, J.; Wang, Z.; et al. Improving relative permittivity and suppressing dielectric loss of triboelectric layers for high-performance wearable electricity generation. *ACS Nano* **2022**, *16* (12), 20251−20262.
(55) Kumar, C.; Perris, J.; Bairagi, S.; Min, G.; Xu, Y.; Gadegaard, N.; Mulvihill, D. M. Multiscale in-situ quantification of the role of surface roughness and contact area using a novel Mica-PVS triboelectric nanogenerator. *Nano Energy* **2023**, *107*, No. 108122.
(56) Sun, J.; Tu, K.; Büchele, S.; Koch, S. M.; Ding, Y.; Ramakrishna, S. N.; Stucki, S.; Guo, H.; Wu, C.; Keplinger, T.; et al. Functionalized wood with tunable tribopolarity for efficient triboelectric nanogenerators. *Matter* **2021**, *4* (9), 3049−3066.
(57) Kwon, D.-H.; Kwon, J.-H.; Jeong, J.; Lee, Y.; Biswas, S.; Lee, D.-W.; Lee, S.; Bae, J.-H.; Kim, H. Textile Triboelectric Nanogenerators with Diverse 3D-Spacer Fabrics for Improved Output Voltage. *Electronics* **2021**, *10* (8), No. 937, DOI: 10.3390/electronics10080937.
(58) Yang, C.-R.; Ko, C.-T.; Chang, S.-F.; Huang, M.-J. Study on fabric-based triboelectric nanogenerator using graphene oxide/porous PDMS as a compound friction layer. *Nano Energy* **2022**, *92*, No. 106791.
(59) Kim, S.; Gupta, M. K.; Lee, K. Y.; Sohn, A.; Kim, T. Y.; Shin, K. S.; Kim, D.; Kim, S. K.; Lee, K. H.; Shin, H. J.; et al. Transparent flexible graphene triboelectric nanogenerators. *Adv. Mater.* **2014**, *26* (23), 3918−3925.
(60) Zhou, Q.; Kim, J.-N.; Han, K.-W.; Oh, S.-W.; Umrao, S.; Chae, E. J.; Oh, I.-K. Integrated dielectric-electrode layer for triboelectric nanogenerator based on Cu nanowire-Mesh hybrid electrode. *Nano Energy* **2019**, *59*, 120−128.
(61) Seyedin, S.; Razal, J. M.; Innis, P. C.; Jeiranikhameneh, A.; Beirne, S.; Wallace, G. G. Knitted strain sensor textiles of highly conductive all-polymeric fibers. *ACS Appl. Mater. Interfaces* **2015**, *7* (38), 21150−21158.
(62) Gunawardhana, K. R. S.; Wanasekara, N. D.; Wijayantha, K. G.; Dharmasena, R. D. I. Scalable Textile Manufacturing Methods for Fabricating Triboelectric Nanogenerators with Balanced Electrical and Wearable Properties. *ACS Appl. Electron. Mater.* **2022**, *4* (2), 678−688.
(63) Huang, T.; Zhang, J.; Yu, B.; Yu, H.; Long, H.; Wang, H.; Zhang, Q.; Zhu, M. Fabric texture design for boosting the performance of a knitted washable textile triboelectric nanogenerator as wearable power. *Nano Energy* **2019**, *58*, 375−383.
(64) Wang, T.; Shen, Y.; Chen, L.; Wang, K.; Niu, L.; Liu, G.; He, H.; Cong, H.; Jiang, G.; Zhang, Q.; Ma, P.; Chen, C. Large-scale production of the 3D warp knitted terry fabric triboelectric nanogenerators for motion monitoring and energy harvesting. *Nano Energy* **2023**, *109*, No. 108309.
(65) Liu, Z.; Chen, K.; Fernando, A.; Gao, Y.; Li, G.; Jin, L.; Zhai, H.; Yi, Y.; Xu, L.; Zheng, Y.; Li, H.; Fan, Y.; Li, Y.; Zheng, Z. Permeable graphited hemp fabrics-based, wearing-comfortable pressure sensors for monitoring human activities. *Chem. Eng. J.* **2021**, *403*, No. 126191.
(66) Zhang, D.; Yang, W.; Gong, W.; Ma, W.; Hou, C.; Li, Y.; Zhang, Q.; Wang, H. Abrasion resistant/waterproof stretchable triboelectric yarns based on fermat spirals. *Adv. Mater.* **2021**, *33* (26), No. 2100782.

https://doi.org/10.1021/acsapm.3c02087
ACS Appl. Polym. Mater. 2024, 6, 407−418